ACS OMEGA

Article

Cite This: *ACS Omega* 2019, 4, 19840−19846

http://pubs.acs.org/journal/acsodf

Nanostructured Hybrid-Material Transparent Surface with Antireflection Properties and a Facile Fabrication Process

Juan Rombaut,[†] Manuel Fernandez,[†] Prantik Mazumder,[‡] and Valerio Pruneri*[,†,§]

[†]ICFO—Institut de Ciències Fotòniques, The Barcelona Institute of Science and Technology, 08860 Castelldefels, Barcelona, Spain
[‡]Corning Research and Development Corporation, Sullivan Park, Corning, 14831 New York, United States
[§]ICREA—Institució Catalana de Recerca i Estudis Avançats, 08010 Barcelona, Spain

Supporting Information

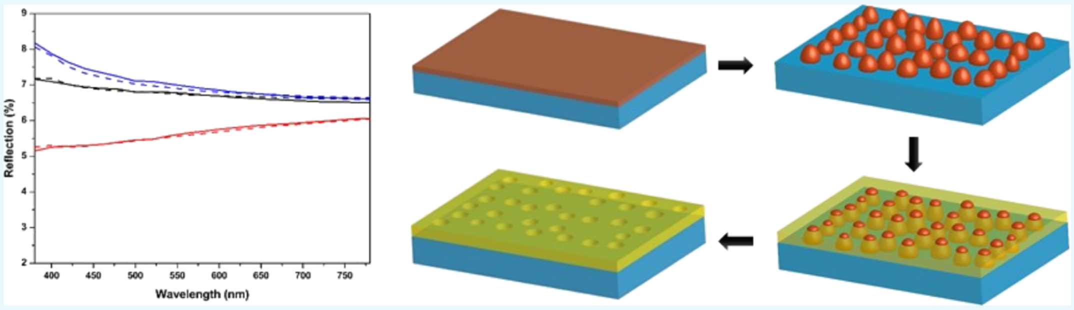

ABSTRACT: Highly transparent optical surfaces with antireflection (AR) properties have the potential to increase the performance of a wide range of applications, such as windows for photovoltaic cells, photodetectors, and display screens among others. Biomimetic structures inspired by the moth-eye have attracted much attention as they can offer superior AR properties, which can generate broadband, omnidirectional optical transmission, and water-repellent self-cleaning behavior. However, many biomimetic surfaces suffer from time-consuming and complex processing, for example, electron beam and nanoimprint lithography, and/or sub-optimal mechanical reliability. In this paper, we introduce a hybrid material approach—nanostructured polyimide on a substrate—for demonstrating a surface with significant AR and hydrophobic properties together with low scattering (haze) and high mechanical resistance. As an example of applications, we demonstrate an indium tin oxide transparent conductive substrate with a large AR effect and optical transmission associated to the nanostructured polyimide coating. The proposed design and method based on conventional spin-coating and lithography-free metal dewetting have the potential to be a low-cost processing path of nanostructured AR transparent substrates.

INTRODUCTION

Optical surfaces made of transparent materials such as glass, quartz, dielectric crystals, and organic polymers suffer from high reflectivity, which negatively impacts the performances of the optical and optoelectronic devices such as lenses, displays, photodetectors, sensors, and solar cells among many others. For example, in the case of glass, a widely used material for optical devices, the reflectivity is typically 4% under normal angle of incidence (AOI) which becomes even larger at higher AOI. Therefore, there have been intensive efforts toward the development of antireflection (AR) technologies over the past decades, for both organic and inorganic substrates including opaque substrates such as silicon wafers. Conventional and commercially available technologies are based on AR coatings, among which the most common approach is based on multilayer coatings. By controlling the thickness and the refractive indices of the layered materials, destructive interference and negligible reflections can be achieved.[1−10] However, simultaneously achieving broadband performance in both wavelength and AOI is challenging with AR multilayers. For large AOI, reflections become significant for a structure designed to work properly at AOI close to 0°.

One alternative is to use subwavelength nanostructured surfaces. In nature, such surfaces are found in the eyes of many nocturnal insects.[11−17] For example, in the case of moths, the surface of each cornea is a hexagonal array of cuticular nanostructures with a conical shape. The subwavelength dimensions ensure little, if any, scattering (haze) while offering a gradual change of the effective refractive index. This leads to the broadband and omnidirectional AR property.[18−22] Similar structures can be encountered on lotus leaves which provide superhydrophobicity and self-cleaning property.[23−28] Unfortunately, many of the proposed technical solutions to produce nanostructured AR surfaces involve time-consuming and expensive lithography (e.g., electron beam and nanoimprint), and often, the mechanical durability of the nanostructures

Received: August 27, 2019
Accepted: October 31, 2019
Published: November 12, 2019

DOI: 10.1021/acsomega.9b02775
ACS Omega 2019, 4, 19840−19846

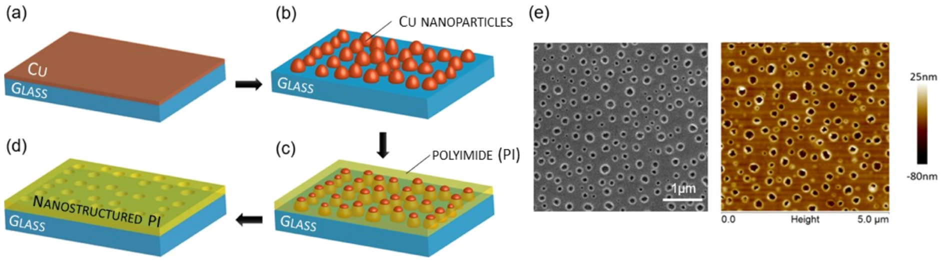

Figure 1. Nanostructured PI fabrication process flow. Ultrathin Cu film is deposited on a glass (FS) substrate by sputtering (a). Thermal dewetting creates Cu nanoparticles (b) that are partially covered with spin-coated PI (c). Finally, the Cu particles are removed by chemical etching leading to a PI nanohole array (d). SEM (left) and AFM (right) images of the final PI nanohole array structure on glass (e).

against abrasion test is not sufficient, and in many instances, it is not even reported.[29−35]

Recently, we reported a method of creating the AR glass substrate through nanoholes.[28] The process entails deposition of polystyrene nanobeads followed by reducing its size by oxygen plasma etching. After deposition of the copper film, reactive ion etching replicate structures in the glass and, finally, the copper mask is removed. Both broadband AR property and mechanical durability have been demonstrated on the glass substrates with nanoholes. In the present paper, we introduce a hybrid material approach, nanostructured polyimide (PI) on the glass substrate as an alternative process that is easier to fabricate. The new approach obviates the need for the glass etching step, while maintaining similar AR and durability properties of the substrate as in the previous work. PI is chosen for its high transparency in the visible wavelength region and high chemical and mechanical resistance.[36−38] In order to nanostructure the PI film, we use metal dewetting, that is, the formation of high surface density nanoparticles from an ultrathin metal film that undergoes a rapid thermal annealing (RTA). Metal dewetting for nanostructuring the surface of glass substrates had already been used by us;[19,39,40] however, to our knowledge, it is the first time that is exploited to nanopattern films of polymers, such as PI. Such technique has the advantage of being simple and scalable as it does not rely on time-consuming and sophisticated lithography (e.g., electron beam and nanoimprint). Nanoimprint technology is often used to create polymer nanostructures on a receiving substrate via molding of an initially deposited film using a proper mask.[29,31] On the contrary, in our work, we first define the Cu nanomask on the substrate and then deposit the polymeric PI film. Finally, the nanostructure is created by simple etching of the Cu nanomask. We have demonstrated the versatility of the current method by creating a nanohole PI film onto glass and indium tin oxide (ITO)-coated glass substrates, which leads to a combined effect of high transparency, low reflectivity, high conductivity, making it a suitable candidate for applications such as transparent heaters. Additionally, we have also developed a numerical model of the optical properties of the hybrid substrate, which enables optimal design.

■ METHODS

Nanohole Patterning of the PI Film on the Glass Substrate. In the last few years, patterning techniques such as nanoimprint lithography (NIL) or microcontact printing (μ-CP) have been investigated for nanostructuring a wide range of polymers. Attempts to nanostructure a thin layer of PI on different substrates have also been reported. Nanostructuring via NIL showed good resolution and throughput. In spite of this, NIL suffers from several shortcomings. If the PI curing is performed during the molding step, lower processing temperatures can be used, but solvent degassing might occur, creating bubbles and damaging the structures. In addition, the demolding step can also distort the shape. If, instead, the NIL template is employed on an already cured PI film, temperatures above glass transition are needed. These typically range from 300 to 500 °C, which could be too high for many materials forming devices. Etching the PI layer using a previously NIL-nanostructured photoresist as a mask can also be considered. Nevertheless, this method is not preferred, as it usually needs additional etching steps or intermediate silica layers between the PI film and the photoresist. In our work, we use the metal dewetting technique to form the initial nanopatterning as it is explained in the following of this section.

The nanostructured PI on glass substrate fabrication steps are shown in Figure 1. Double-side, optically polished, ultraviolet-grade fused silica (FS) glass substrates, with a thickness of 1 mm and an area of 1 inch square, were used. Initially, their surface was cleaned in acetone followed by ethanol in an ultrasonic bath for 10 min each. The substrates were then rinsed in deionized water and dried with nitrogen followed by oxygen plasma cleaning for 10 min (PVA TePla 300 SemiAuto Plasma Asher). Ultrathin copper (Cu) films with a thickness of 15 nm were deposited on the flat glass surface using a magnetron sputtering system (ATC Orion 8, AJA International, Inc.), as shown in Figure 1a. The depositions were performed at a base pressure of 10^{-8} Torr, room temperature, 100 W of DC-power, and 25 standard cubic centimeters per minute of pure argon (Ar). The working pressure was 1.5×10^{-3} Torr, the deposition rate was 0.166 nm/s, and the target−substrate distance was 40 cm. In order to create nanoparticles, the samples were subjected to RTA, as shown in Figure 1b. Dewetting takes place because the surface energy of the ultrathin metal film is greater than the interfacial and surface energy of the underlying substrate. Before RTA, all of the samples were blown with a N_2 gun to ensure that the surface was completely clear of small dust particles and pollutants that could alter the dewetting process. The RTA was carried out in the TsunamiTM RTP-600S system at the temperature of 750 °C for 135 s. High-purity N_2 gas (1 atm pressure) was used to prevent oxidation of the metal film. After RTA, diluted polyimide (CP1 polyimide, NeXolve Materials) in *N*-methyl-2-pyrrolidone (NMP) was spin-coated over the whole sample, but only partially the metal dewetted nanoparticles. An APS [(3-aminopropyl)triethoxysilane] promoter was used to improve the adhesion of the PI layer to the glass substrate.[41] By modifying the concentration of PI in the NMP

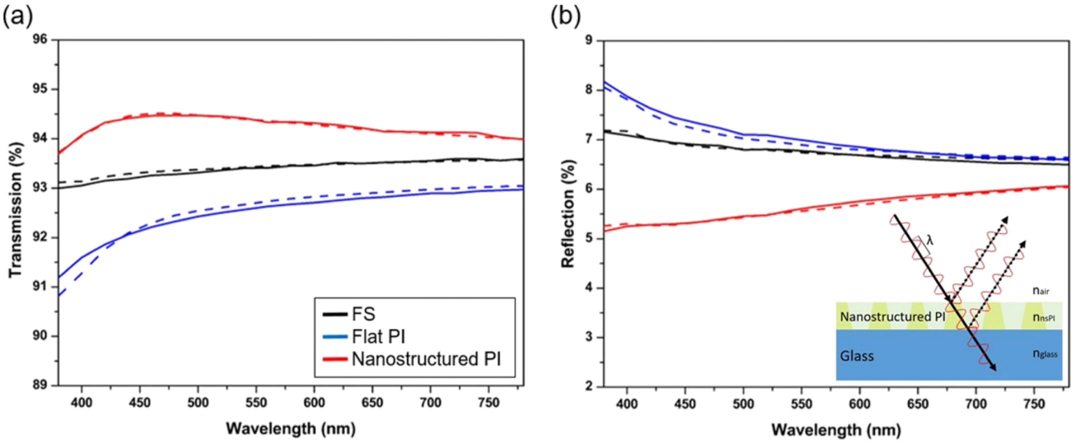

Figure 2. Optical response of the bare FS substrate, flat (continuous) polyimide (flat PI), and nanostructured polyimide (Nanostructured PI) on the same substrate. Measured direct transmission (a) and reflection (b) for the different structures. Experiment (continuous line) and simulation (dashed line). Note that only the front side is coated with PI and nanostructured PI. The inset shows a schematic view of the propagation of light rays through the nanostructured PI. The antireflective effect comes from the destructive interference created by the film, approximating a quarter-wave layer.

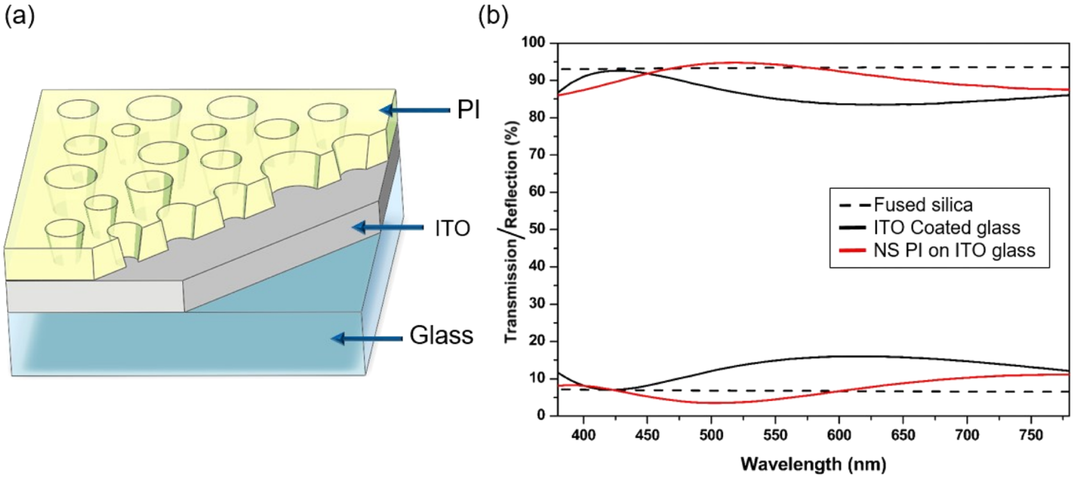

Figure 3. Schematic illustration of the proposed nanostructured polyimide (NS PI) on the ITO-coated glass structure (a). Corresponding optical transmission and reflection. Measurements for glass (Fused silica) and ITO-coated glass substrates are also shown for comparison (b).

solution and some of the parameters of the spin coater (G3P Spin Coater, specialty coating systems), it is possible to control the thickness of the deposited film. Optimal results were achieved with a ratio of 1:3 of PI on NMP, with parameters of 6000 rpm and 90 s for the spin-coating process. The curing process is critical to determine the final PI properties. A two-step curing was performed. First, the samples were cured at 100 °C for 3 min and subsequently at 200 °C for 15 min. Both steps were carried out on a hot plate (Cimarec digital hot plate stirrer, Thermo Scientific). After the curing process, by using ammonium persulfate, it is possible to chemically etch the Cu nanoparticles, leaving a nanohole PI film structure on the surface.

Optical, Morphological, Durability, and Wetting Characterization. The optical transmission and reflection were measured in the wavelength range of 380−800 nm by using a UV−vis−NIR spectrophotometer (PerkingElmer LAMBDA 950). Reflection measurements at normal incidence in Figures 2 and 3 are carried out with an AOI of 6°. Haze measurements were performed using Haze-meter (BYK-Gardner 4601 haze-gloss). Ten measurements per sample were carried out to obtain the average value and the standard deviation. The morphology of the samples was examined by a scanning electron microscope (FEG-SEM, Inspect F, FEI Systems) working from 2 to 5 kV accelerating voltage at 10 mm distance. Additional surface analysis was performed using atomic force microscopy (AFM) (VEECO Dimension 3100, Bruker). The PI thickness was measured using a profilometer (KLA Tencor). The durability test was done by a crockmeter machine (M238BB Electronic Crockmeter, SDL ATLAS). The crockmeter test provides reproducible and comparable results emulating the action of a human finger using standard rubbing materials (microfiber cloth). It uses a constant force (9 N) over 2 cm^2 and is repeated for specific number of cycles. It is a standard test standardized by the American Association of Textile Chemists and Colorists (AATCC) as test method 8. The wetting properties of the samples were determined by measuring the static and dynamic water contact angle by using a drop shape analysis system (DSA-100, Krüss GmbH). Different areas of each sample were examined and averaged.

Modeling of Optical Response. Finite element method commercial software (COMSOL Multiphysics) was used to perform electromagnetic simulations. The nanostructured PI on glass was simulated using periodic boundary conditions and

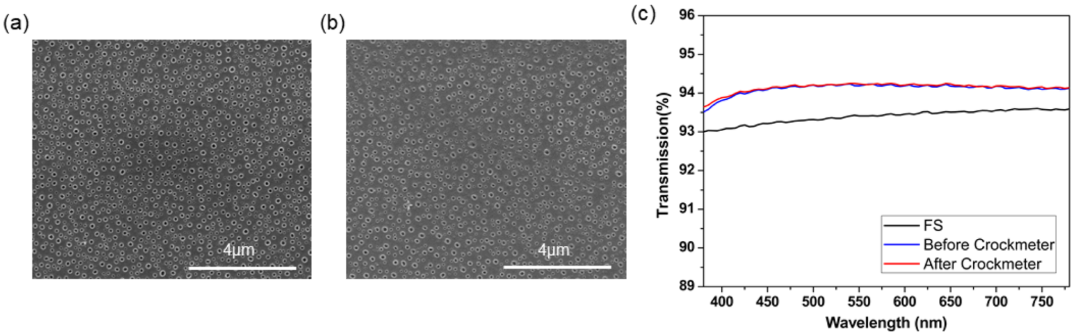

Figure 4. Mechanical durability using the crockmeter test of nanostructured PI on the glass (FS) substrate (sample similar to that of Figure 2). Comparison between before (a) and after (b) more than 500 passes performed with standard 9 N force over 2 cm^2 contact area using the standard microfiber crockmeter cloth. Optical comparison of bare FS and nanostructured PI on the FS substrate before and after the crockmeter test (c).

modeled as a square cell with a centered cavity. Parametric sweep to optimize the structure was performed using dimensional analysis from SEM and profilometer measurements (Supporting Information, Figure 2a). Refractive index and absorption coefficients of PI (Supporting Information, Figure S2b1) were calculated from the best fit of experimental transmission and reflection results of the flat (continuous) PI film on the FS substrate. The FS refractive index plotted in Supporting Information, Figure S2b2, is taken from the Filmetrics.com refractive index database.

■ RESULTS AND DISCUSSION

The new method to fabricate subwavelength nanostructures in PI films is shown in Figure 1 and described in detail in the Methods section. The initial ultrathin Cu film deposited by sputtering (Figure 1 a) determines the size, height, and density of the Cu nanoparticles (nanoholes in the final PI film) formed after the dewetting process represented in Figure 1 b. The thicker the initial Cu film, the larger the size of nanoholes and lower their surface density in the final nanostructured PI film. We performed simulations that confirmed that deviations in nanohole size and density with respect to those of the nanostructured PI on the glass sample of Figure 2 lead to a lower AR effect and transmission for the PI thickness used in the paper. The thickness of the PI and the height of the metal nanoparticles are key factors to create the nanostructure successfully. If the metal nanoparticles are too short or the PI film is too thick, the former remains embedded in the latter and cannot be removed by etching (see Supporting Information, Figure S1).

Figure 2 shows the total transmission and reflection as a function of wavelength for bare glass, continuous PI, and nanostructured PI on glass. All the samples had the same PI thickness (60 nm) determined from profilometry. Because of the refractive index and absorption coefficient of PI, the addition of a continuous film reduced transmission and increased reflection of the coated FS substrate. After nanohole formation in the PI film, AR effects are clearly visible (Figure 2b), with transmission becoming larger than the initial FS substrate (Figure 2a). The incident light is reflected from both the top surface of the nanostructured PI film and interface between the nanostructured PI film and substrate. The reflected light beams interfere, and when the thickness of the PI film gets close to a quarter of the wavelength, the interference becomes destructive, thus minimizing the reflection (inset of Figure 2b). The PI film has subwavelength nanostructures (nanoholes); this leading to an effective refractive index given by the volume ratio between air/PI. The effective refractive index determines the thickness that corresponds to the quarter-wave layer condition. Despite the fact that the quarter-wave layer condition is not completely achieved because of the lithographic limit of the PI thickness, our results are comparable with other polymer-based AR solutions[42−44] or nanostructured films on polymeric substrates[45] but without the need for using molding or lithography processes. In the future, full optimization should improve current performance even further.

In Figure 2, we also show results from full-wave electromagnetic simulations using a commercial finite element package (COMSOL Multiphysics Modeling Software). The refractive index and absorption coefficient for PI for the simulation are shown in Supporting Information, Figure S2, and are obtained through the best fit of the experimental response of the continuous (flat) PI on the FS substrate. The average period (200 nm), diameter (135 nm), and angle (30°) of the nanohole PI structure were extracted from a statistical analysis of SEM images. There is a good agreement between experiment and simulation, which is essential for design optimization. We also simulated the angular dependence of the AR response of the nanostructured PI film on the FS substrate and on ITO on the FS substrate (Supporting Information, Figure S3), confirming that one-side reflection remains below 7 and 16%, respectively, up to an AOI of 60°.

A crucial parameter for optical surfaces is light scattering, usually quantified through the haze factor. In many applications, haze must maintain a low value. For example, the haze value is preferred to be less than 1% in display applications. The average haze value and standard deviation for our nanostructured PI on FS were 0.07 and 0.02%, respectively, very close to the detection limit of the instrument. This confirms that reflected and transmitted light are essentially direct, with very little scattering. The decrease in transmission at shorter wavelength is likely due to absorption in the PI layer.

The proposed hybrid-material surface nanostructuring process is versatile and could be applied to a large variety of substrate materials for different applications. As a prototypical example, we show its use for the ITO-coated glass (FS) substrate. ITO-based transparent conductive surfaces are the key in many optoelectronic devices, where electrical signals need to be generated or collected with high optical transmission, for example, light-emitting diodes, solar cells, smart windows, and liquid crystal displays. The nanostructuring of the PI film was carried out in the same way as it was described in the Methods section for the glass (FS) substrate. The ITO thickness was 100 nm. As it is shown in Figure 3, the AR effects are significant, leading to a strongly reduced reflection over almost the entire visible wavelength range, and correspondingly, a transmission larger than the initial ITO on the glass substrate. At the same time, the entire process essentially maintains the electrical conductivity of the ITO layer (lower than 20 Ω/sq).

Next, we investigated the mechanical durability of the nanostructured substrate. Figure 4 shows the effect of the crockmeter test on the proposed hybrid PI glass nanostructured surface. As it can be seen from comparing SEM images and the optical characterization before and after more than 500 crock-meter passes, the PI nanostructure remains practically unchanged. The proven surface durability is because of the well-known PI mechanical strength as well as the fact that the bonding force between the PI film and FS substrate was increased by using an adhesion promoter (3-aminopropyl) triethoxysilane (APTES). The mechanical resistance test indicates a strong adhesion between the nanostructured PI film and the underneath substrate, especially considering the fact that nanostructuring reduces the surface available for the adhesion of the PI to the substrate and may also weaken the cohesive strength of the film. In the case of the nanostructured PI on the ITO-coated glass substrate, the PI also acts as a protective layer for the ITO, maintaining its electrical conductivity. Besides being strong, the PI film is mechanically flexible. Therefore, the proposed nanostructured PI film can be easily applied to flexible substrates, such as ultrathin glass.[46]

The wetting property on the nanohole surface could be described by the well-known Cassie−Baxter equation

$$\cos\theta = f\cos\theta_1 + (1 - f)\cos\theta_2 \qquad (1)$$

where θ is the contact angle of the composite state, f is the area fraction of the holes, θ_1 and θ_2 are the Young contact angles on the hole and solid areas. As it is shown in Figure 5, the bare glass (FS) coated with continuous (flat) PI shows a water contact angle of about $\theta_2 = 95°$. After nanostructuring the PI film, the underlying substrate could be clean glass for which the Young contact angle could be very low. In the limiting case of ultraclean glass, $\theta_1 = 0°$, the contact angle of the composite state according to eq 1 is $\theta \approx 74°$ approximately, corresponding to $f = 0.33$. This is the reason behind reduction of the contact angle after nanoholes are formed. However, after the flurosilanization step, the Young contact angle of the glass is $\theta_1 = 120°$. There is uncertainty with respect to where the droplet meniscus resides in this configuration. However, the contact angle for the two limiting cases could be calculated: (1) meniscus fully wets the holes and (2) meniscus is suspended on the hole. The contact angles for these two limiting cases according to eq 1 are approximately 103 and 113°. We note that larger contact angles are required to achieve superhydrophobicity and eventually self-cleaning properties. In the future, this may be possible by increasing the void fraction of the current nanohole structure and the chemical affinity between the fluorosilane coating and the PI material.[47]

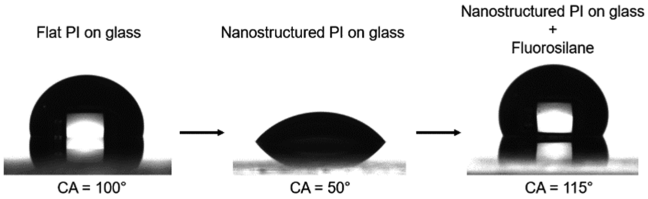

Figure 5. Wetting characterization. Comparison between the bare glass (FS) substrate with flat PI, nanostructured PI, and nanostructured PI coated with fluorosilane.

CONCLUSIONS

We have proposed a hybrid material-nanostructured optical surface, namely, a PI film with nanohole geometry, which possess significant AR properties, together with low scattering, high transparency, and mechanical durability. It can be fabricated using inexpensive, lithography-free, and scalable metal dewetting techniques. The combination of all these features make the newly developed optical surface relevant for a wide range of applications such as windows for photovoltaic cells, photodetectors, display screens, and optical components for remote sensing. As an example, which could be utilized to fabricate transparent heaters, we have demonstrated that the optical performance of a commercially available transparent and conductive ITO-coated glass substrate can be effectively improved without affecting the electrical properties by applying the proposed nanostructured PI film.

ASSOCIATED CONTENT

Supporting Information

The Supporting Information is available free of charge on the ACS Publications website at DOI: 10.1021/acsomega.9b02775.

> Key factor during the fabrication process, SEM and AFM images, nanocavity structure with the refractive index used, simulations of the angular dependence of the AR response of the nanostructured PI film, and cross-sectional SEM image of the structure (PDF)

AUTHOR INFORMATION

Corresponding Author

*E-mail: valerio.pruneri@icfo.eu.

ORCID

Juan Rombaut: 0000-0002-6438-0765

Author Contributions

The manuscript was written through contributions of all authors. All authors have given approval to the final version of the manuscript.

Notes

The authors declare no competing financial interest.

ACKNOWLEDGMENTS

We acknowledge financial support from the Spanish Ministry of Economy and Competitiveness through the “Severo Ochoa” program for Centres of Excellence in R&D (SEV-2015-0522), from Fundació Privada Cellex, and from Generalitat de Catalunya trough the CERCA program.

REFERENCES

(1) Rayleigh, L. On Reflection of Vibrations at the Confines of two Media between which the Transition is Gradual. *Proc. London Math. Soc.* **1879**, *s1–s11*, 51–56.

(2) Born, M.; Wolf, E. *Principles of Optics*, 4th ed.; Pergamon Press: Oxford, 1970.

(3) Macleod, H. *Thin-Film Optical Filters*, 4th ed.; CRC Press: Bristol, 2010.

(4) Dobrowolski, J. A.; Poitras, D.; Ma, P.; Vakil, H.; Acree, M. Toward Perfect Antireflection Coatings: Numerical Investigation. *Appl. Opt.* **2002**, *41*, 3075.

(5) Raut, H. K.; Ganesh, V. A.; Nair, A. S.; Ramakrishna, S. Anti-Reflective Coatings: A Critical, in-Depth Review. *Energy Environ. Sci.* **2011**, *4*, 3779.

(6) Hedayati, M. K.; Elbahri, M. Antireflective Coatings: Conventional Stacking Layers and Ultrathin Plasmonic Metasurfaces, a Mini-Review. *Materials (Basel).* **2016**, *9*, 497.

(7) Khan, S. B.; Wu, H.; Huai, X.; Zou, S.; Liu, Y.; Zhang, Z. Mechanically Robust Antireflective Coatings. *Nano Res.* **2018**, *11*, 1699−1713.

(8) Buskens, P.; Burghoorn, M.; Mourad, M. C. D.; Vroon, Z. Antireflective Coatings for Glass and Transparent Polymers. *Langmuir* **2016**, *32*, 6781−6793.

(9) Shimomura, H.; Gemici, Z.; Cohen, R. E.; Rubner, M. F. Layer-by-Layer-Assembled High-Performance Broadband Antireflection Coatings. *ACS Appl. Mater. Interfaces* **2010**, *2*, 813−820.

(10) Schallenberg, U. B. Antireflection Design Concepts with Equivalent Layers. *Appl. Opt.* **2006**, *45*, 1507.

(11) Parker, A. R.; Townley, H. E. Biomimetics of Photonic Nanostructures. *Nat. Nanotechnol.* **2007**, *2*, 347−353.

(12) Han, Z. W.; Wang, Z.; Feng, X. M.; Li, B.; Mu, Z. Z.; Zhang, J. Q.; Niu, S. C.; Ren, L. Q. Antireflective Surface Inspired from Biology : A Review. *Biosurface and Biotribology* **2016**, *2*, 137−150.

(13) Pan, Z.; Cheng, F.; Zhao, B. Bio-Inspired Polymeric Structures with Special Wettability and Their Applications : An Overview. *Polymers* **2017**, *9*, 725.

(14) Chen, J. Y.; Chang, W.-L.; Huang, C. K.; Sun, K. W. Biomimetic Nanostructured Antireflection Coating and Its Application on Crystalline Silicon Solar Cells. *Opt. Express* **2011**, *19*, 14411−14419.

(15) Oh, S. S.; Choi, C.-G.; Kim, Y.-S. Fabrication of Micro-Lens Arrays with Moth-Eye Antireflective Nanostructures Using Thermal Imprinting Process. *Microelectron. Eng.* **2010**, *87*, 2328−2331.

(16) Diao, Z.; Hirte, J.; Chen, W.; Spatz, J. P. Inverse Moth Eye Nanostructures with Enhanced Antireflection and Contamination Resistance. *ACS Omega* **2017**, *2*, 5012−5018.

(17) Ji, S.; Song, K.; Nguyen, T. B.; Kim, N.; Lim, H. Optimal Moth Eye Nanostructure Array on Transparent Glass towards Broadband Antireflection. *ACS Appl. Mater. Interfaces* **2013**, *5*, 10731−10737.

(18) Mazumder, P.; Jiang, Y.; Baker, D.; Carrilero, A.; Tulli, D.; Infante, D.; Hunt, A. T.; Pruneri, V. Superomniphobic, Transparent, and Antireflection Surfaces Based on Hierarchical Nanostructures. *Nano Lett.* **2014**, *14*, 4677−4681.

(19) Tulli, D.; Hart, S. D.; Mazumder, P.; Carrilero, A.; Tian, L.; Koch, K. W.; Yongsunthon, R.; Piech, G. A.; Pruneri, V. Monolithically Integrated Micro- and Nanostructured Glass Surface with Antiglare, Antireflection, and Superhydrophobic Properties. *ACS Appl. Mater. Interfaces* **2014**, *6*, 11198−11203.

(20) Khan, S. B.; Wu, H.; Xie, Z.; Wang, W.; Zhang, Z. Al 2 O 3 Encapsulated Teflon Nanostructures with High Thermal Stability and Efficient Antireflective Performance. *ACS Appl. Mater. Interfaces* **2017**, *9*, 36327−36337.

(21) Cai, J.; Qi, L. Recent Advances in Antireflective Surfaces Based on Nanostructure Arrays. *Mater. Horiz.* **2015**, *2*, 37−53.

(22) Liapis, A. C.; Rahman, A.; Black, C. T. Self-Assembled Nanotextures Impart Broadband Transparency to Glass Windows and Solar Cell Encapsulants. *Appl. Phys. Lett.* **2017**, *111*, 183901.

(23) Barthlott, W.; Neinhuis, C. Purity of the Sacred Lotus, or Escape from Contamination in Biological Surfaces. *Planta* **1997**, *202*, 1−8.

(24) Ensikat, H. J.; Ditsche-Kuru, P.; Neinhuis, C.; Barthlott, W. Superhydrophobicity in Perfection: The Outstanding Properties of the Lotus Leaf. *Beilstein J. Nanotechnol.* **2011**, *2*, 152−161.

(25) Gao, L.; McCarthy, T. J. The "Lotus Effect" Explained: Two Reasons Why Two Length Scales of Topography Are Important. *Langmuir* **2006**, *22*, 2966−2967.

(26) Bhushan, B.; Nosonovsky, M. The Rose Petal Effect and the Modes of Superhydrophobicity. *Philos. Trans. R. Soc., A* **2010**, *368*, 4713−4728.

(27) Jeevahan, J.; Chandrasekaran, M.; Britto Joseph, G.; Durairaj, R. B.; Mageshwaran, G. Superhydrophobic Surfaces: A Review on Fundamentals, Applications, and Challenges. *J. Coat. Technol. Res.* **2018**, *15*, 231−250.

(28) Rombaut, J.; Maniyara, R. A.; Bellman, R. A.; Acquard, D. F.; Baca, A. S.; Osmond, J.; Senaratne, W.; Quesada, M. A.; Baker, D.; Mazumder, P.; et al. Antireflective Transparent Oleophobic Surfaces by Noninteracting Cavities. *ACS Appl. Mater. Interfaces* **2018**, *10*, 43230−43235.

(29) Gonzalez-Martinez, I. G.; Bachmatiuk, A.; Bezugly, V.; Kunstmann, J.; Gemming, T.; Liu, Z.; Cuniberti, G.; Rümmeli, M. H. Electron-Beam Induced Synthesis of Nanostructures: A Review. *Nanoscale* **2016**, *8*, 11340−11362.

(30) Chou, S. Y. Nanoimprint Lithography. *J. Vac. Sci. Technol. B* **1996**, *14*, 4129.

(31) Zhou, W.; Min, G.; Zhang, J.; Liu, Y.; Wang, J.; Zhang, Y.; Sun, F. Nanoimprint Lithography: A Processing Technique for Nanofabrication Advancement. *Nano-Micro Lett.* **2011**, *3*, 135−140.

(32) Nie, Z.; Kumacheva, E. Patterning Surfaces with Functional Polymers. *Nat. Mater.* **2008**, *7*, 277−290.

(33) Fukukawa, K.-i.; Ueda, M. Recent Progress of Photosensitive Polyimides. *Polym. J.* **2008**, *40*, 281−296.

(34) Chiu, C.-Y.; Lee, Y.-C. Fabrication of Polyimide Micro/Nano-Structures Based on Contact-Transfer and Mask-Embedded Lithography. *J. Micromech. Microeng.* **2009**, *19*, 105001.

(35) Cui, B.; Cortot, Y.; Veres, T. Polyimide Nanostructures Fabricated by Nanoimprint Lithography and Its Applications. *Microelectron. Eng.* **2006**, *83*, 906−909.

(36) Liaw, D.-J.; Wang, K.-L.; Huang, Y.-C.; Lee, K.-R.; Lai, J.-Y.; Ha, C.-S. Advanced Polyimide Materials: Syntheses, Physical Properties and Applications. *Prog. Polym. Sci.* **2012**, *37*, 907−974.

(37) Xu, C.-L.; Wang, Y.-Z. Durability, Anti-Corrosion and Self-Clean in Air/Oil of a Transparent Superhydrophobic Polyimide Film. *Appl. Mater. Today* **2018**, *10*, 18−23.

(38) Cosutchi, A. I.; Hulubei, C.; Dorohoi, D. O.; Neagu, M.; Ioan, S. Optical Surface Properties of Polyimides Cross-Linked Thin Film. *Rom. Rep. Phys.* **2008**, *53*, 755−760.

(39) Infante, D.; Koch, K. W.; Mazumder, P.; Tian, L.; Carrilero, A.; Tulli, D.; Baker, D.; Pruneri, V. Durable, Superhydrophobic, Antireflection, and Low Haze Glass Surfaces Using Scalable Metal Dewetting Nanostructuring. *Nano Res.* **2013**, *6*, 429−440.

(40) Mazumder, P.; Jiang, Y.; Baker, D.; Carrilero, A.; Tulli, D.; Infante, D.; Hunt, A. T.; Pruneri, V. Superomniphobic, Transparent, and Antire Fl Ection Surfaces Based on Hierarchical Nanostructures. *Nano Lett.* **2014**, *14*, 4677−4681.

(41) Marchena, M.; Wagner, F.; Arliguie, T.; Zhu, B.; Johnson, B.; Fernández, M.; Chen, T. L.; Chang, T.; Lee, R.; Pruneri, V.; Mazumder, P. Dry Transfer of Graphene to Dielectrics and Flexible Substrates Using Polyimide as a Transparent and Stable Intermediate Layer. *2D Mater.* **2018**, *5*, 035022.

(42) Cho, J.-H.; Park, J.-H.; Lee, M.-H.; Song, H.-K.; Lee, S.-Y. A Polymer Electrolyte-Skinned Active Material Strategy toward High-Voltage Lithium Ion Batteries: A Polyimide-Coated LiNi0.5Mn1.5O4 Spinel Cathode Material Case. *Energy Environ. Sci.* **2012**, *5*, 7124.

(43) Zhang, J.; Shen, S.; Dong, X. X.; Chen, L. S. Low-Cost Fabrication of Large Area Sub- Wavelength Anti-Reflective Structures on Polymer Film Using a Soft PUA Mold. *Opt. Express* **2014**, *22*, 1842−1851.

(44) Daglar, B.; Khudiyev, T.; Demirel, G. B.; Buyukserin, F.; Bayindir, M. Soft Biomimetic Tapered Nanostructures for Large-Area Antireflective Surfaces and SERS Sensing. *J. Mater. Chem. C* **2013**, *1*, 7842−7848.

(45) Ai, L.; Zhang, J.; Li, X.; Zhang, X.; Lu, Y.; Song, W. Universal Low-Temperature Process for Preparation of Multifunctional High-Performance Antireflective Mesoporous Silica Coatings on Trans-

parent Polymeric Substrates. *ACS Appl. Mater. Interfaces* **2018**, *10*, 4993.

(46) Formica, N.; Mantilla-Perez, P.; Ghosh, D. S.; Janner, D.; Chen, T. L.; Huang, M.; Garner, S.; Martorell, J.; Pruneri, V. An Indium Tin Oxide-Free Polymer Solar Cell on Flexible Glass. *ACS Appl. Mater. Interfaces* **2015**, *7*, 4541−4548.

(47) Gu, H. Y.; Qi, Z. Y.; Wu, W.; Zeng, Y.; Song, L. X. Superhydrophobic Polyimide Films with High Thermal Endurance via UV Photo-Oxidation. *eXPRESS Polym. Lett.* **2014**, *8*, 588−595.